# Metal Oxide Nanocrystals from the Injection of Metal Oxide Sols in a Coordinating Environment: Principles, Applicability, and Investigation of the Synthesis Variables in the Case Study of $CeO_2$ and $SnO_2$

Mauro Epifani,*[,†] Eva Pellicer,[‡,§] Jordi Arbiol,[‡,∥] and Joan R. Morante[‡,⊥]

*Consiglio Nazionale delle Ricerche, Istituto per la Microelettronica ed i Microsistemi (C.N.R.-I.M.M.), via Monteroni, I-73100 Lecce, Italy, EME/XaRMAE/IN2UB, Departament d'Electrònica, Universitat de Barcelona, C. Martí i Franquès 1, 08028 Barcelona, CAT, Spain, MIND-IN2UB, Departament d'Electrònica, Universitat de Barcelona, Martí i Franques 1, 08028 Barcelona, CAT, Spain, TEM-MAT, Serveis Cientificotecnics, Universitat de Barcelona, Sole i Sabaris 1-3, 08028 Barcelona, CAT, Spain, and Institut de Recerca en Energia de Catalunya (IREC), C/Josep Pla 2, 08019 Barcelona, Spain*

*Received December 5, 2008*

Metal oxide sols (ZnO, $SnO_2$, $TiO_2$, $ZrO_2$, $Fe_2O_3$, NiO, $Ga_2O_3$, $MnO_2$, $In_2O_3$, $CeO_2$) were prepared by hydrolysis of chloro-alkoxo or acetylacetonato complexes, preventing precipitation. The sols were injected in a solution of tetradecene and an aliphatic amine at 160 °C and heated at the resulting temperature for 3 h, resulting in the formation of metal oxide nanoparticles. The crystallization degree of the resulting nanoparticles depended on the particular system, and nanocrystals were obtained for ZnO, $SnO_2$, $Fe_2O_3$, $Ga_2O_3$, $In_2O_3$, $CeO_2$ systems. The chemical features of the process were investigated on $SnO_2$ and $CeO_2$ as case systems, by X-ray diffraction, transmission electron microscopy, Fourier transform infrared spectroscopy, and nuclear magnetic resonance. The initial hypothesis that the amine present in the injection solution may act at the same time as a catalyst of the inorganic condensation reactions and as a growth stopper by bonding to the surface metal atoms of the nanoparticles, was thoroughly investigated and it resulted that the alkylamine structure and the processing of the starting sol can influence the nanocrystal formation pathway. In particular, bulkier amines favor the formation of smaller nanocrystals, whereas favoring the condensation reactions in the starting sols results in larger nanocrystals.

## Introduction

The wet chemical procedures to metal oxide nanocrystals are in a very rapidly developing stage,[1] and an increasing number of systems have been synthesized. A description of the currently available synthesis procedures can be carried out according to different criteria, for instance, depending on the synthesis conditions. In this case, a broad discrimination occurs between syntheses carried out in solvothermal conditions[2] and those using controlled heating of the precursors in normal pressure conditions.[3] The first group includes such systems as $CeO_2$,[4] cobalt oxides,[5] $Cu_2O$,[6] perovskites,[7] $\gamma$-$Al_2O_3$,[8] Mn oxides,[9] multiferroics,[10] $SnO_2$,[11] $TiO_2$,[12] $WO_3$,[2b,13] $In_2O_3$,[2a,11b] indium−tin oxide,[14] iron oxides,[15] ZnO,[2a] $Y_2O_3$,[16] $Ta_2O_5$ and $HfO_2$,[17] $ZrO_2$,[18] etc. High-temperature decomposi-

* Corresponding author. mauro.epifani@le.imm.cnr.it.
† Consiglio Nazionale delle Ricerche, Istituto per la Microelettronica ed i Microsistemi.
‡ Departament d'Electrònica, Universitat de Barcelona.
§ Current address: Departament de Física, Universitat Autònoma de Barcelona, E-08193 Bellaterra, Spain.
∥ TEM-MAT, Serveis Cientificotecnics, Universitat de Barcelona.
⊥ Institut de Recerca en Energia de Catalunya (IREC).

(1) (a) Yun, Y.-w.; Choi, J.-s.; Cheon, J. *Angew. Chem., Int. Ed.* **2006**, *45*, 3414–3439. (b) Niederberger, M. *Acc. Chem. Res.* **2007**, *40*, 793–800. (c) Rao, C. N. R.; Müller, A.; Cheetam, A. K. *Nanomaterials Chemistry: Recent Developments and New Directions*; Wiley-VCH: Weinheim, Germany, 2007; (d) Rao, C. N. R.; Vivekchand, S. R. C.; Biswas, K.; Govindaraj, A. *Dalton Trans.* **2007**, 3728–3749. (e) Park, J.; Joo, J.; Kwon, S. G.; Jang, Y.; Hyeon, T. *Angew. Chem., Int. Ed.* **2007**, *46*, 4630–4660. (f) Niederberger, M.; Pinna, N. *Angew. Chem., Int. Ed.* **2008**, *47*, 5292–5304.

(2) (a) Pinna, N.; Garnweitner, G.; Antonietti, M.; Niederberger, M. *J. Am. Chem. Soc.* **2005**, *127*, 5608–5612. (b) Niederberger, M.; Bartl, M. H.; Stucky, G. D. *J. Am. Chem. Soc.* **2002**, *124*, 13642–13643.

(3) (a) Rockenberger, J.; Scher, E. C.; Alivisatos, A. P. *J. Am. Chem. Soc.* **1999**, *121*, 11595–11596. (b) Feldmann, C. *Adv. Funct. Mater.* **2003**, *13*, 101–107. (c) Park, J.; An, K.; Hwang, Y.; Park, J.-G.; Noh, H.-J.; Kim, J.-Y.; Park, J.-H.; Hwang, N.-M.; Hyeon, T. *Nat. Mater.* **2004**, *3*, 891–895. (d) Jana, N. R.; Chen, Y.; Peng, X. *Chem. Mater.* **2004**, *16*, 3931–3935. (e) Seo, J.-w.; Yun, Y.-w.; Ko, S. J.; Cheon, J. *J. Phys. Chem. B* **2005**, *109*, 5389–5391. (f) Jun, Y.-W.; Choi, J.-S.; Cheon, J. *Angew. Chem., Int. Ed.* **2006**, *45*, 3414–3439.

(4) (a) Zhang, Y.-W.; Si, R.; Liao, C.-S.; Yan, C.-H.; Xiao, C.-X.; Kou, Y. *J. Phys. Chem. B* **2003**, *107*, 10159–10167. (b) Si, R.; Zhang, Y.-W.; You, L.-P.; Yan, C.-H. *J. Phys. Chem. B* **2006**, *110*, 5994–6000. (c) Mai, H.-X.; Sun, L.-D.; Zhang, Y.-W.; Si, R.; Feng, W.; Zhang, H.-P.; Liu, H.-C.; Yan, C.-H. *J. Phys. Chem. B* **2005**, *109*, 24380–24385. (d) Vantomme, A.; Yuan, Z.-Y.; Du, G.; Su, B.-L. *Langmuir* **2005**, *21*, 1132–1135. (e) Yang, S.; Gao, L. *J. Am. Chem. Soc.* **2006**, *128*, 9330–9331. (f) Zhang, J.; Ohara, S.; Umetsu, M.; Naka, T.; Hatakeyama, Y.; Adschiri, T. *Adv. Mater.* **2007**, *19*, 203–206. (g) Zhou, F.; Zhao, X.; Xu, H.; Yuan, C. *J. Phys. Chem. C* **2007**, *111*, 1651–1657.

(5) (a) Ghosh, M.; Sampathkumaran, E. V.; Rao, C. N. R. *Chem. Mater.* **2005**, *17*, 2348–2352. (b) He, T.; Chen, D.; Jiao, X.; Wang, Y. *Adv. Funct. Mater.* **2006**, *18*, 1078–1082.

(6) Chang, Y.; Teo, J. J.; Zeng, H. C. *Langmuir* **2005**, *21*, 1074–1079.

(7) (a) Niederberger, M.; Garnweitner, G.; Pinna, N.; Antonietti, M. *J. Am. Chem. Soc.* **2004**, *126*, 9120–9126. (b) Niederberger, M.; Pinna, N.; Polleux, J.; Antonietti, M. *Angew. Chem., Int. Ed.* **2004**, *43*, 2270–2273. (c) Garnweitner, G.; Hentschel, J.; Antonietti, M.; Niederberger, M. *Chem. Mater.* **2005**, *17*, 4594–4599.

(8) Zhou, S.; Antonietti, M.; Niederberger, M. *Small* **2007**, *3*, 763–767.

(9) Cheng, F.; Zhao, J.; Song, W.; Li, C.; Ma, H.; Chen, J.; Shen, P. *Inorg. Chem.* **2006**, *45*, 2038–2044. (b) Djerdj, I.; Arcon, D.; Jaglicic, Z.; Niederberger, M. *J. Phys. Chem. C* **2007**, *111*, 3614–3623.

10.1021/cm803282k CCC: $40.75 
Published on Web 02/09/2009

tion or sol−gel processing of metal oxide precursors has allowed the preparation of nanocrystalline iron oxides,[3a,19] $CeO_2$,[20] CoO,[21] CuO,[22] perovskites,[23] pigments and other functional oxides,[3b,24] manganese oxides,[25] $In_2O_3$,[26] NiO,[27] $SnO_2$,[28] rare earth oxides,[29] spinels,[30] $TiO_2$,[31] $ZrO_2$,[32] ZnO.[33] On the other hand, a unifying feature of all these procedures is the direct processing of molecular precursors. We have recently shown that an alternative synthetic concept can be developed by processing nonmolecular precursors,[34] consisting in simple metal oxide sols. The sols are prepared in such a way to hinder extensive inorganic cross-linking, which was supposed to result in mild crystallization conditions. The nanoparticles preparation then required the injection of the sols in a solution of tetradecene and an aliphatic amine at moderate temperatures (about 160 °C), followed by heating at the resulting temperature (80−100 °C) for 3 h. The amine had the role of both promoting the inorganic cross-linking of the oxide species in the sol and at the same time acting as a ligand so preventing excessive growth. The whole development allowed obtaining several metal oxide nanocrystals ($SnO_2$, ZnO, $In_2O_3$, $TiO_2$) in mild conditions. After these early developments, some questions remained open:

(i) What should be concluded about the generality of the process? Are the obtained products always crystalline? This second question is related to the effectiveness of the peculiar sol preparation process in improving the crystallization degree.[34]

(ii) Is it possible to gain a general view of the nanoparticle formation pathways and to control the particle size by understanding the synthesis process?

In this work,we provide our answers to such questions and the resulting further perspectives. The second part of


(10) Han, J. T.; Huang, Y.-H.; Huang, W.; Goodenough, J. B. *J. Am. Chem. Soc.* **2006**, *128*, 14454–14455.

(11) (a) Zhang, D.-F.; Sun, L.-D.; Yin, J.-L.; Yan, C.-H. *Adv. Mater.* **2003**, *15*, 1022–1025. (b) Pinna, N.; Neri, G.; Antonietti, M.; Niederberger, M. *Angew. Chem., Int. Ed.* **2004**, *43*, 2–5. (c) Cheng, B.; Russell, J. M.; Shi, W.; Zhang, L.; Samulski, E. T. *J. Am. Chem. Soc.* **2004**, *126*, 5972–5973. (d) Ba, J.; Polleux, J.; Antonietti, M.; Niederberger, M. *Adv. Mater.* **2005**, *17*, 2509–2512.

(12) (a) Wang, C.-C.; Ying, J. Y. *Chem. Mater.* **1999**, *11*, 3113–3120. (b) Aruna, S. T.; Tirosh, S.; Zaban, A. *J. Mater. Chem.* **2000**, *10*, 2388–2391. (c) Wu, M.; Lin, G.; Chen, D.; Wang, G.; He, D.; Feng, S.; Xu, R. *Chem. Mater.* **2002**, *14*, 1974–1980. (d) Niederberger, M.; Bartl, M. H.; Stucky, G. D. *Chem. Mater.* **2002**, *14*, 4364–4370. (e) Pan, D.; Zhao, N.; Wang, Q.; Jiang, S.; Ji, X.; An, L. *Adv. Mater.* **2005**, *17*, 1991–1995. (f) Tahir, M. N.; Theato, P.; Oberle, P.; Melnyk, G.; Faiss, S.; Kolb, U.; Janshoff, A.; Stepputat, M.; Tremel, W. *Langmuir* **2006**, *22*, 5209–5212. (g) Wang, X. M.; Xiao, P. *J. Mater. Res.* **2006**, *21*, 1189–1203.

(13) Polleux, J.; Gurlo, A.; Barsan, N.; Weimar, U.; Antonietti, M.; Niederberger, M. *Angew. Chem., Int. Ed.* **2006**, *45*, 261–265.

(14) Ba, J.; Fattakhova Rohlfing, D.; Feldhoff, A.; Brezesinski, T.; Djerdj, I.; Wark, M.; Niederberger, M. *Chem. Mater.* **2006**, *18*, 2848–2854.

(15) (a) Pinna, N.; Grancharov, S.; Beato, P.; Bonville, P.; Antonietti, M.; Niederberger, M. *Chem. Mater.* **2005**, *17*, 3044–3049. (b) Wu, C.; Yin, P.; Zhu, X.; OuYang, C.; Xie, Y. *J. Phys. Chem. B* **2006**, *110*, 17806–17812. (c) Wang, S.-B.; Min, Y.-L.; Yu, S.-H. *J. Phys. Chem. C* **2007**, *111*, 3551–3554.

(16) Pinna, N.; Garnweitner, G.; Beato, P.; Niederberger, M.; Antonietti, M. *Small* **2005**, *1*, 112–121.

(17) Pinna, N.; Garnweitner, G.; Antonietti, M.; Niederberger, M. *Adv. Mater.* **2004**, *16*, 2196–2200.

(18) Zhao, N.; Pan, D.; Nie, W.; Ji, X. *J. Am. Chem. Soc.* **2006**, *128*, 10118–10124.

(19) (a) Hyeon, T.; Lee, S. S.; Park, J.; Chung, Y.; Na, H. B. *J. Am. Chem. Soc.* **2001**, *123*, 12798–12801. (b) Sun, S.; Zeng, H. *J. Am. Chem. Soc.* **2002**, *124*, 8204–8205. (c) Yu, W. W.; Falkner, J. C.; Yavuz, C. T.; Colvin, V. L. *Chem. Commun.* **2004**, 2306–2307. (d) Cheon, J.; Kang, N.-J.; Lee, S.-M.; Lee, J.-H.; Yoon, J.-H.; Oh, S. J. *J. Am. Chem. Soc.* **2004**, *126*, 1950–1951. (e) Redl, X. F.; Black, C. T.; Papaefthymiou, G. C.; Sandstrom, R. L.; Yin, M.; Zeng, H.; Murray, C. B.; O'Brien, S. P. *J. Am. Chem. Soc.* **2004**, *126*, 14583–14599. (f) Lee, Y.; Lee, J.; Bae, C. J.; Park, J. G.; Noh, H.-J.; Park, J.-H.; Hyeon, T. *Adv. Funct. Mater.* **2005**, *15*, 503–509. (g) Park, J.; Lee, E.; Hwang, N.-M.; Kang, M.; Kim, S. C.; Hwang, Y.; Park, J.-G.; Noh, H.-J.; Kim, J.-Y.; Park, J.-H.; Hyeon, T. *Angew. Chem., Int. Ed.* **2005**, *44*, 2872–2877. (h) Cozzoli, P. D.; Snoeck, E.; Garcia, M. A.; Giannini, C.; Guagliardi, A.; Cervellino, A.; Gozzo, F.; Hernando, A.; Achterhold, K.; Ciobanu, N.; Parak, F. G.; Cingolani, R.; Manna, L. *Nano Lett.* **2006**, *6*, 1966–1972.

(20) (a) Yu, T.; Joo, J.; Park, Y. I.; Hyeon, T. *Angew. Chem., Int. Ed.* **2005**, *44*, 7411–7414. (b) Gu, H.; Soucek, M. D. *Chem. Mater.* **2007**, *19*, 1103–1110.

(21) An, K.; Lee, N.; Park, J.; Kim, S. C.; Hwang, Y.; Park, J.-G.; Kim, J.-Y.; Park, J.-H.; Han, M. J.; Yu, J.; Hyeon, T. *J. Am. Chem. Soc.* **2006**, *128*, 9753–9760.

(22) Yin, M.; Wu, C.-K.; Lou, Y.; Burda, C.; Koberstein, J. T.; Zhu, Y.; O'Brien, S. *J. Am. Chem. Soc.* **2005**, *127*, 9506–9511.

(23) O'Brien, S.; Brus, L.; Murray, C. B. *J. Am. Chem. Soc.* **2001**, *123*, 12085–12086.

(24) (a) Feldmann, C. *Adv. Funct. Mater.* **2001**, *13*, 1301–1303. (b) Feldmann, C.; Jungk, H.-O. *Angew. Chem., Int. Ed.* **2001**, *40*, 359–362.

(25) (a) Yin, M.; O'Brien, S. *J. Am. Chem. Soc.* **2003**, *125*, 10180–10181. (b) Park, J.; Kang, E.; Bae, C. J.; Park, J.-G.; Noh, H.-J.; Kim, J.-Y.; Park, J.-H.; Park, H. M.; Hyeon, T. *J. Phys. Chem. B* **2004**, *108*, 13594–13598. (c) Zitoun, D.; Pinna, N.; Frolet, N.; Belin, C. *J. Am. Chem. Soc.* **2005**, *127*, 15034–15035. (d) Zhong, X.; Xie, R.; Sun, L.; Lieberwirth, I.; Knoll, W. *J. Phys. Chem. B* **2006**, *110*, 2–4. (e) Wang, N.; Guo, L.; He, L.; Cao, X.; Chen, C.; Wang, R.; Yang, S. *Small* **2007**, *3*, 606–610.

(26) (a) Seo, W. S.; Jo, H. H.; Lee, K.; Park, J. T. *Adv. Mater.* **2003**, *15*, 795–797. (b) Liu, Q.; Lu, W.; Ma, A.; Tang, J.; Lin, J.; Fang, J. *J. Am. Chem. Soc.* **2005**, *127*, 5276–5277. (c) Lee, C. H.; Kim, M.; Kim, T.; Kim, A.; Paek, J.; Lee, J. W.; Choi, S. Y.; Kim, K.; Park, J.-B.; Lee, K. *J. Am. Chem. Soc.* **2006**, *128*, 9326–9327. (d) Narayasnaswami, A.; Xu, H.; Pradhan, N.; Kim, M.; Peng, X. *J. Am. Chem. Soc.* **2006**, *128*, 10310–10319.

(27) Park, J.; Kang, E.; Son, S. U.; Park, H. M.; Lee, M. K.; Kim, J.; Noh, H.-J.; Park, J.-H.; Bae, C. J.; Park, J.-G.; Hyeon, T. *Adv. Mater.* **2005**, *17*, 429–434.

(28) Epifani, M.; Arbiol, J.; Diaz, R.; Peralvarez, M. J.; Siciliano, P.; Morante, J. R. *Chem. Mater.* **2005**, *17*, 6468–6472.

(29) (a) Cao, Y. C. *J. Am. Chem. Soc.* **2004**, *126*, 7456–7457. (b) Si, R.; Zhang, Y.-W.; You, L.-P.; Yan, C.-H. *Angew. Chem., Int. Ed.* **2005**, *44*, 3256–3260. (c) Wang, H.; Uehara, M.; Nakamura, H.; Miyazaki, M.; Maeda, H. *Adv. Mater.* **2005**, *17*, 2506–2509. (d) Si, R.; Zhang, Y.-W.; Zhou, H.-P.; Sun, L.-D.; Yan, C.-H. *Chem. Mater.* **2007**, *19*, 18–27.

(30) (a) Caruntu, D.; Remond, Y.; Chou, N. H.; Jun, M.-J.; Caruntu, G.; He, J.; Goloverda, G.; O'Connor, C.; Kolesnichenko, V. *Inorg. Chem.* **2002**, *41*, 6137–6146. (b) Hyeon, T.; Chung, Y.; Park, J.; Lee, S. S.; Kim, Y.-W.; Park, B. H. *J. Phys. Chem. B* **2002**, *106*, 6831–6833. (c) Song, Q.; Zhang, Z. J. *J. Am. Chem. Soc.* **2004**, *126*, 6164–6168. (d) Kang, E.; Park, J.; Hwang, Y.; Kang, M.; Park, J.-G.; Hyeon, T. *J. Phys. Chem. B* **2004**, *108*, 13932–13935.

(31) (a) Trentler, T. J.; Denler, T. E.; Bertone, J. F.; Agrawal, A.; Colvin, V. L. *J. Am. Chem. Soc.* **1999**, *121*, 1613–1614. (b) Cozzoli, P. D.; Kornowski, A.; Weller, H. *J. Am. Chem. Soc.* **2003**, *125*, 14539–14548. (c) Tang, J.; Redl, F.; Zhu, Y.; Siegrist, T.; Brus, L. E.; Steigerwald, M. L. *Nano Lett.* **2005**, *5*, 543–548. (d) Koo, B.; Park, J.; Kim, Y.; Choi, S.-H.; Sung, Y.-E.; Hyeon, T. *J. Phys. Chem. B* **2006**, *110*, 24318–24323.

(32) (a) Joo, J.; Yu, T.; Kim, Y. W.; Park, H. M.; Wu, F.; Zhang, J. Z.; Hyeon, T. *J. Am. Chem. Soc.* **2003**, *125*, 6553–6557. (b) Mizuno, M.; Sasaki, Y.; Lee, S.; Katakura, H. *Langmuir* **2006**, *22*, 7137–7140.

(33) (a) Shim, M.; Guyot-Sionnest, P. *J. Am. Chem. Soc.* **2001**, *123*, 11651–11654. (b) Cozzoli, P. D.; Curri, M. L.; Agostiano, A.; Leo, G.; Lomascolo, M. *J. Phys. Chem. B* **2003**, *107*, 4756–4762. (c) Yin, M.; Gu, Y.; Kuskovski, I. L.; Andelman, T.; Zhu, Y.; Neumark, G. F.; O'Brien, S. *J. Am. Chem. Soc.* **2004**, *126*, 6206–6207. (d) Kahn, M. L.; Monge, M.; Colliere, V.; Senocq, F.; Maisonnat, A.; Chaudret, B. *Adv. Funct. Mater.* **2005**, *15*, 458–468. (e) Cheng, Y.; Kim, M.; Lian, G.; Johnson, M. B.; Peng, X. *J. Am. Chem. Soc.* **2005**, *127*, 13331–13337. (f) Choi, S.-H.; Kim, E.-G.; Park, J.; An, K.; Lee, N.; Kim, S. C.; Hyeon, T. *J. Phys. Chem. B* **2005**, *109*, 14792–14794. (g) Joo, J.; Kwon, S. G.; Yu, J. H.; Hyeon, T. *Adv. Mater.* **2005**, *17*, 1873–1877.

(34) Epifani, M.; Díaz, R.; Arbiol, J.; Comini, E.; Sergent, N.; Pagnier, T.; Siciliano, P.; Faglia, G.; Morante, J. R. *Adv. Funct. Mater.* **2006**, *16*, 1488–1498.

the work was carried out by analyzing the effect of the processing parameters on $CeO_2$ and $SnO_2$ as case systems. It will be shown that (i) the applicability of the process has to be verified for each particular metal oxide, because of the crystallization behavior of each system. The presence of many tunable synthetic parameters allows keeping open the synthesis of those systems not yet attainable; (ii) the nanocrystals form by a self-arrested sol−gel precipitation pathway, influenced by the structure and concentration of the amine and the processing of the starting sol; this knowledge helps in establishing the conditions for controlling the nanocrystal size.

## Experimental Section

**(1) Chemicals.** Metal nitrates ($Zn(NO_3)_2 \cdot 6H_2O$, $Fe(NO_3)_3 \cdot 9H_2O$, $Ni(NO_3)_2 \cdot 6H_2O$, $Ga(NO_3)_3 \cdot xH_2O$, $Mn(NO_3)_2 \cdot xH_2O$, $In(NO_3)_3 \cdot 5H_2O$, $Ce(NO_3)_3 \cdot 6H_2O$), and anhydrous metal chlorides ($SnCl_4$, $TiCl_4$, $ZrCl_4$) were purchased from Sigma-Aldrich. All the solvents for the sol preparation or processing (see below) together with acetylacetone (acacH) were purchased from Sigma-Aldrich in analytical grade and used without any further purification. The amines tested throughout the work were *n*-dodecylamine, *n*-hexylamine, hexadecylamine, all purchased from Sigma-Aldrich and used without any further purification. In the following, they will be indicated with DA, HA, HDA, respectively.

**(2) Metal Oxide Sol Preparation.** *(a) Nitrate Precursors.* For each metal nitrate, 2.6 mmol was dissolved in 10 mL (15 mL for Zn and In) of methanol. Only for Zn was 4.4 mmol of the nitrate used. Acetylacetone was added to the resulting clear solution with an acacH:metal molar ratio that in the following will be denoted with $R_{ac}$. In the case of the $Ga_2O_3$ sol, the nitrate was slowly dissolved by stirring for 24 h in a solution of acetylacetone in 10 mL of methanol with $R_{ac} = 2.9$. After 1 h since the addition of acacH, a 30 wt % ammonia solution in water was dropped in the metal complexes solutions, followed by vigorous stirring for further 24 h. The $NH_3$:metal molar ratio will be indicated in the following with $R_B$. Only in two cases, for $CeO_2$ and $In_2O_3$ syntheses, did precipitation occurred for very high $R_B$ values. In these cases, after 24 h of vigorous stirring of the precipitate, concentrated (65 wt % solution in water) nitric acid was added until complete dissolution of the precipitate.

*(b) Chloride Precursors.* For each metal chloride, 3.9 mmol was reacted with 10 mL of methanol in a glovebox, with evolution of heat and vapors. One hour after methanol addition, water was added, with a $H_2O$:metal molar ratio that in the following will be denoted with $R_w$. After water addition, the sol remained clear and colorless, and only for very high $R_w$ values did it became opalescent. It was vigorously stirred for 24 h after water addition. In no case was precipitation observed in the resulting solutions.

**(3) Nanoparticle Preparation by Metal Oxide Sol Processing.** In a 500 mL flask, thoroughly degassed with nitrogen, a solution of an amine in 10 mL of tetradecene was poured. The amine volume in milliliters will be denoted with $V_A$, where A is the previously defined amine symbol. The solution was then heated up to 160 °C, and 2 mL of a metal oxide sol were injected in the flask. In the case of $SnO_2$ sols with $R_W$ of 64, 2.5 mL were injected in order to compensate the sol dilution due to the higher water concentration used in the preparation of the latter. The solution temperature dropped to 80−100 °C, depending on the system, and was kept at such a value by decreasing the power supply to the flask heater. After a given time from the injection step, the flask was cooled. Methanol or isopropanol were added to the resulting slurry, eventually followed by toluene, in order to overcome any phase separation and to improve the extraction efficiency of the nanoparticles. The slurry was centrifuged, and the precipitate was washed with hexane and shortly dried at 80 °C in air. The yield of the various processes was about 70−80% of the theoretical value, and the synthesis scale ranged from 30 (e.g., $In_2O_3$) to 80 mg (e.g., $SnO_2$), depending on the system.

**(4) Materials Characterization.** X-ray diffraction (XRD) patterns of the dried or heat-treated powders were obtained with a Siemens D-500 X-ray diffractometer using the radiation emitted by a Cu cathode ($\lambda = 1.5418$ Å), with an operating voltage of 40 kV and a current of 30 mA. Data were collected in steps of 0.05° ($2\theta$) from 20 to 80°.

The specific surface area of selected systems heat-treated at 500 °C was measured by the Brunauer−Emmett−Teller (BET) method, with an ASAP 2020 Micromeritics system. Before the analysis, the sample were degassed for 10 h at 175 °C.

The Fourier transform infrared (FTIR) spectroscopic measurements were carried out with a Bomem MB-120 FTIR spectrometer, in a spectral range from 350 to 4000 $cm^{-1}$. The samples were prepared by mixing a dried nanocrystal aliquot with KBr and then preparing pellets.

The structural and morphological characterization of the dried nanoparticles was carried out by means of transmission electron microscopy (TEM) and selected area electron diffraction (SAED). To obtain the high-resolution TEM (HRTEM) results, we used a field-emission gun microscope Jeol 2010F, which works at 200 kV and has a point-to-point resolution of 0.19 nm. The software used for digital image analysis and crystallographic indexation was the Digital Micrograph (Gatan) and Carine, respectively. The samples for the TEM observations were prepared by placing a drop of nanocrystals suspensions in hexane onto a carbon-coated copper grid, followed by drying.

$^{119}Sn$ NMR spectra on the starting $SnO_2$ sols were measured with a Varian Gemini 300 MHz spectrometer. $^1H$ NMR spectra of the synthesis byproduct were measured with a Varian Inova 300 MHz or Varian Gemini 300 MHz spectrometers. Chemical shifts are referred to tetramethylsilane (TMS). The synthesis byproduct were biphasic and the upper phases were diluted in $CDCl_3$, whereas the lower ones were diluted in $CD_3OD$.

N,C,H,S determination on dried $SnO_2$ and $CeO_2$ nanocrystals was carried out by using a Carlo Erba model EA 1108 elemental analyzer.

## Results and Discussion

**(1) General Features of the Synthetic Route.** The sol processing was examined in some of the peculiar aspects, in order to establish the range within which the parameters could be changed. Some qualitative features readily emerged: (i) the use of an amine in the injection stage is necessary, since injection of the sol in the pure solvent resulted in the formation of carbonaceous products, in a poorly crystallized unidentified phase; (ii) the requirement of limiting the cross-linking reactions in the sol preparation appeared as unavoidable, because the processing of sols prepared by simple precipitation-peptization procedures resulted in small yields in the form of waxy products, amorphous or in unidentified phases; (iii) the injection temperature was kept at 160 °C because at room temperature the metal oxide sol and the amine solution in tetradecene were immiscible. Temperatures higher than 160 °C could result in uncontrolled decompositions. Finally, when the injection occurred at 160 °C, the resulting temperature of the reaction pot was sufficient to

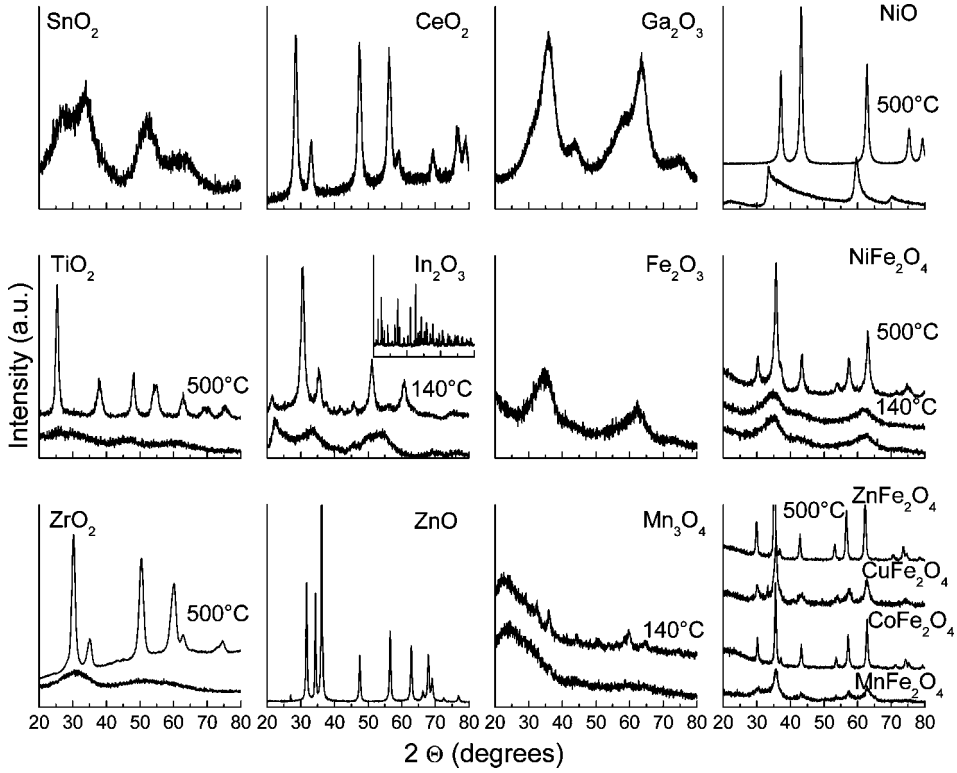


**Figure 1.** XRD patterns recorded on the indicated systems, synthesized with the parameters described in the text. Where the temperature is not indicated, the patterns are related to materials synthesized at 80−100 °C. The insert in the $In_2O_3$ pattern is related to a synthesis with a sol prepared without acetylacetone. The $2\theta$ range is the same for all the reported patterns.

**Table 1. Synthesis Parameters for the Nitrate-Derived Nanoparticles in Figure 1**

| | Nitrate Precursor | | |
|---|---|---|---|
| oxide | $R_{ac}$ | $R_B$ | $V_{DA}$ |
| $CeO_2$ | 3 | 0.6 | 1 |
| $In_2O_3$ | 3 | 4.2 | 1 |
| ZnO | 0.2 | 0 | 1 |
| $Ga_2O_3$ | 3 | 1.8 | 0.6[a] |
| $Fe_2O_3$ | 3 | 2 | 1 |
| $Mn_3O_4$ | 3 | 1 | 1 |
| NiO | 3 | 2 | 0.6[a] |
| ferrites | 3[b] | 1.4[b] | 1 |

[a] HA was used instead of DA. [b] With respect to the (Fe+ Me) total number of moles, where Me is the other metal cation (Ni, Co, Cu, Mn, Zn).

obtain crystalline products in many systems. For these reasons, 160 °C was kept as the standard injection temperature; (iv) the sol preparation procedures were suggested by our previous studies[35] showing that the limitation of the extent of cross-linking in the starting sols can be obtained by using acetylacetone in nitrate-derived sols or relying on the residual chlorine in chloride-derived sols.

**(2) Generality of the Synthesis.** In Figure 1, the XRD patterns are reported for metal oxide nanoparticles prepared according to the parameters reported in Table 1. For $SnO_2$, $TiO_2$, and $ZrO_2$, injection in tetradecene/dodecylamine solutions was carried out with $V_{DA} = 1$, whereas the starting solutions were prepared with $R_W = 16$. The crystalline phase for each pattern is reported in the Supporting Information (Table S1). From the results in Figure 1, we observe that a large number of systems can be prepared by just changing the metal salt in the general processing and that where a poorly crystallized product is obtained soon after the synthesis, it is generally related to the most stable crystallographic phase, as evidenced by the heat-treatment at 500 °C.

Data on $In_2O_3$ and $Mn_3O_4$ show that when a poorly crystallized product is obtained, it is likely due to kinetic factors that can be overcome by increasing the processing temperature. In the case of iron oxide, TEM observations confirmed the presence of very small (mean size 3.5 nm) $\alpha$-$Fe_2O_3$ nanocrystals. Magnetic spinels can be also prepared. The extension to such systems as $Y_2O_3$, lead oxides, other rare earth oxides beyond $CeO_2$ seems possible by the similarity of such systems to others already prepared. On the other hand, it is not easy to make predictions about perovskites, because of the kinetic and precursor solubility factors that can be involved in the preparation of complex oxides. We have experimentally tested the possibility of preparing Cu, Cr, V, Mo, and W oxides, observing that by applying the synthetic routes similar to those useful for other systems (by using anhydrous chlorides for V, Mo, and W and nitrates for Cu and Cr) we do not obtain any product (Cu, Cr) or a completely amorphous material that upon heat treatment results in large oxide particles.

For completeness, the BET specific surface area was measured for selected systems after heat treatment at 500 °C, with the values reported in Table 2.

(35) (a) Epifani, M.; Alvisi, M.; Mirenghi, L.; Leo, G.; Siciliano, P.; Vasanelli, L. *J. Am. Ceram. Soc.* **2001**, *84*, 48–54. (b) Epifani, M.; Capone, S.; Rella, R.; Siciliano, P.; Vasanelli, L.; Faglia, G.; Nelli, P.; Sberveglieri, G. *J. Sol-Gel Sci. Tech.* **2003**, *26*, 741–744. (c) Epifani, M.; Siciliano, P.; Gurlo, A.; Barman, N.; Weimar, U. *J. Am. Chem. Soc.* **2004**, *126*, 4078–4079.

**Table 2. BET Specific Surface Area Values ($m^2/g$) for Selected Oxides and Related Nanoparticles Size**

| oxide | BET area | nanoparticle |
|---|---|---|
| $ZrO_2$ | 83.1 | 12.7 |
| $Fe_2O_3$ | 10.8 | 105.8 |
| $CeO_2$ | 80.1 | 9.8 |
| $SnO_2$ | 50.0 | 17.4 |
| $Ga_2O_3$ | 79.2 | 12.6 |
| $TiO_2$ | 63.2 | 22.4 |

The obtained values are very high and justify the use of these materials as gas sensors in our previous work[34] (the low value for iron oxide is due to the substantial grain growth shown by the related XRD pattern). The mean nanoparticles size calculated from the BET data are higher than those obtained from XRD and TEM analysis of selected samples, indicating the aggregation of the initial nanocrystals. On the other hand, the sizes are 2−3 times the TEM values, indicating limited sintering and aggregation.

**(3) Crystalline and Amorphous Products.** From the observation of Figure 1, it results that the peculiar sol processing, by hindering of the condensation reactions, is not always able to overcome the kinetic barrier to crystallization for all the systems, as supposed in our previous work.[34] By observing the inset in the $In_2O_3$ pattern, related to a synthesis with a sol processed by precipitation-peptization, it appears that the sol modification is essential for obtaining a product structurally related to the final oxide. Moreover, although in the literature the synthesis of $SnO_2$ and ZnO nanocrystals is reported in quite mild conditions, the synthesis of $CeO_2$, $Ga_2O_3$, $Mn_3O_4$, and $In_2O_3$ nanocrystals requires more severe conditions than in our work and the patterns related to $In_2O_3$ and $Mn_3O_4$ prepared at 140 °C indicate that the kinetic barrier might be overcome by a moderate increase in the synthesis temperature.We thus conclude this section by abandoning the idea that the condensation hindering in the sol can be a general key to nanocrystals, because of the remaining importance of kinetic factors, but it is a general, very mild and simple method giving suitable precursors for subsequent nanocrystal formation and in several cases results in direct nanocrystal synthesis.

**(4) Investigation of the Chemical Features of the Process.** After the modified sol is prepared, the processing by injection is meant to condense the species in the sol but stopping the condensation at a certain point, in order to remain within the nanosized range. For this reason, the injection solution contained a long chain amine: although the basic properties of the amine allow catalysis of the condensation reaction between the oxide species in the sol, its function as a ligand toward surface metal atoms should keep the particles separated. To investigate the various effects of the amine and the other synthesis parameters on the nanoparticles formation, we choose two case systems: $CeO_2$ for nitrate-derived systems and $SnO_2$ for the chloride-based ones. The idea was that despite the fact that each metal ion may influence the overall mechanism by its chemical peculiarities, it could be possible to draw from the two systems some general laws, to be eventually complemented by specific considerations for each system. The choice of the two systems was suggested by their easy crystallization in a broad range of mild conditions, so constantly providing a ready result evaluation by XRD.

*(a) Search for Chemical Processes Different from the Sol−Gel Chemistry.* The whole nanoparticles processing is based on hydrolytic sol−gel chemistry, so the first step in the process investigation was the search for species indicating the eventual presence of other processes. This investigation was carried out on both the dried nanoparticles and, more importantly, on the liquid byproduct of the synthesis.

(i) FTIR Studies on the Dried Nanoparticles and NMR Studies on the Synthesis Byproduct. In the FTIR spectra measured on various as-prepared materials, a common general structure was evident. The identification of the bands revealed that there were no components apart from the initial reactants. Because the extraction of the nanoparticles from the reaction liquor at the end of the process could remove any noncomplexing species, the liquid byproducts were analyzed by NMR.

$SnO_2$ and $CeO_2$ nanocrystal syntheses were carried out prepared like samples of Figure 1 and with $V_{DA} = 1$. The heating times after injection were 5 and 60 min, in order to have different pictures of the reactant evolution during the early steps of the heating process. The reaction liquid was not extracted during the synthesis; because of its phase separation, no representative samples could be extracted and the whole reaction could be perturbed with respect to the standard protocol. Thus, after the given heating times, the whole flask was cooled and the nanoparticles extracted by centrifugation. For this task, the solvent volumes used for nanoparticles extraction were minimized, in order to decrease any possible interference with the synthesis liquid. The spectra corresponding to both the upper and lower phases of the $CeO_2$ and $SnO_2$ liquids are reported in detail the Supporting Information (Figure S-NMR). No additional signals from newly formed species are observed.

The whole of these results then indicates a formation mechanism in which the initial reactants do not produce new molecular species and that is then in full agreement with the general view of a process based on the simple steps of sol−gel chemistry.

(ii) Crystallization Rate during the Early Processing Stage. It seemed of interest to investigate even the synthesis solid products in the early stages of the processing, in relationship with their crystallization behavior. Thus the XRD patterns were measured on the dried nanoparticles corresponding to the samples analyzed by NMR, and the results are shown in Figure 2. A heating time of 15 min was also considered. It is astonishing that after a few minutes the nanocrystal formation is complete, and although the $SnO_2$ XRD patterns show an evolution of the peak resolution with the heating time, in the case of $CeO_2$, the pattern of the nanoparticles prepared with 5 min of heating shows the presence of a nanocrystalline product. This result is interpreted as a confirmation of the starting hypothesis that the processing of preformed oxide species may substantially lower the crystallization barrier.

We have already seen that this result is not achieved for all the systems, depending on the specific crystallization kinetics, but now it is clear that the peculiar processing of

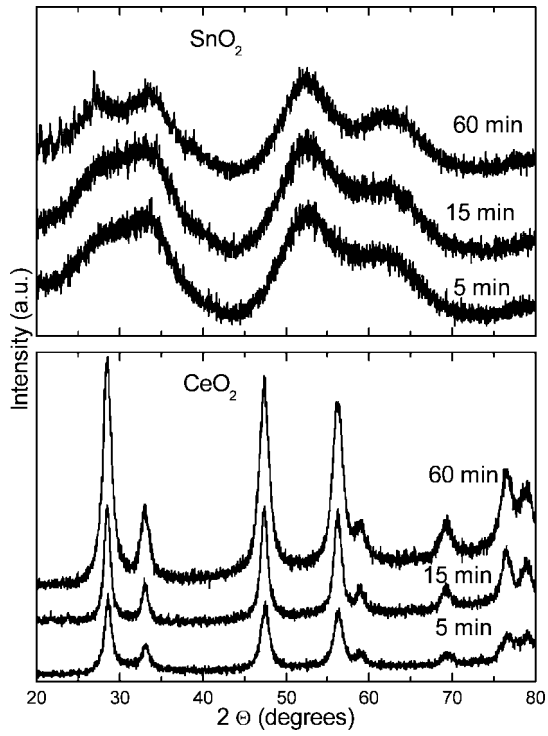


**Figure 2.** XRD patterns recorded on $SnO_2$ nanocrystals prepared with $R_W = 16$ and $V_{DA} = 1$ and $CeO_2$ nanocrystals prepared with $R_{ac} = 3$, $R_B = 0.6$, and $V_{DA} = 1$. The indicated heating times were applied after injection.

metal oxide sols may introduce much favorable crystallization pathways. The very fast formation rate at such low processing temperature indicates that mass transport phenomena are not relevant during the nanoparticles formation process. In fact, the insolubility of the methanol-based sol in the reaction medium could play a much more important role in determining, soon after the injection, isolated regions of the sol that are rapidly condensed. In this way there is no kinetic control in the process, which explains the lack of crystallization for many systems.

*(b) Effect of the Synthesis Parameters.*

(i) Time Evolution of the Growth. One of the roles of amine was the limiting of particle growth phenomena, and this result was verified with samples prepared with different reaction times. For $CeO_2$, the synthesis parameters were the same of Table 1, whereas for $SnO_2$, $R_W = 64$ and $V_{HA} = 0.6$ were used. This choice for $SnO_2$ was motivated by the need for enhancing the effects of particle growth, for which high water concentrations and shorter amines are more favorable, as shown below. The related XRD patterns are shown in Figure S1 of the Supporting Information, because no obvious differences were observed between the various patterns. The mean nanocrystal size deduced from the Scherrer analysis of the lowest angle peak changes, in the case of $CeO_2$, was between 8.6 and 9.0 nm when heating for 3 and 11 h, respectively.

The same occurred for $SnO_2$, where the nanocrystal size ranges around 2.7 nm when heating from 3 to 11 h, without obvious changes. Only after heating for 22 h does the $SnO_2$ nanocrystal size grow to 3.4 nm. This result is readily explained because such a sample was brownish-black after synthesis, revealing the occurrence of organic decompositions. Thus, the corresponding growth is interpreted as the consequence of the loss of the growth hindered by HA because of its decomposition. It is concluded that the growth time is not a critical parameter, once the minimum crystallization time is provided. TEM observations were carried out on the samples heated for 3 h, in order to have a direct imaging of the synthesis products. The results are shown in Figure 3 for $CeO_2$ and in Figure 4 for $SnO_2$ nanocrystals. The samples are partially aggregated, which is a typical effect due to the insufficient capping by residual amine, but they appear as composed by single nanocrystals, generally defect-free and in the crystallographic phases reported in Table S1 of the Supporting Information. The mean size as deduced from a careful analysis of several images, where the crystalline planes of different nanocrystals could be clearly discriminated, was $5.0 \pm 2.0$ nm for $CeO_2$ and $2.7 \pm 0.2$ nm for $SnO_2$. There is a very good agreement between the TEM and XRD data for the $SnO_2$ sample, whereas the XRD data for $CeO_2$ overestimate the size. This typical effect is a consequence of the aggregation of the $CeO_2$ nanocrystals if compared to the $SnO_2$ sample, resulting in a larger crystal domain probed by the XRD beam. Reference to the XRD size in the following will be made with this caution.

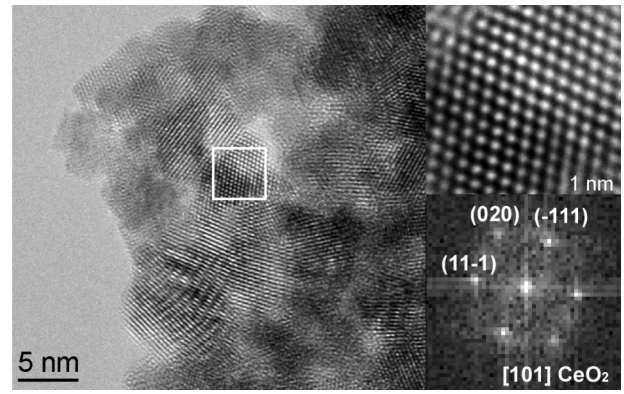


**Figure 3.** General view, HRTEM image, and power spectra of $CeO_2$ nanocrystals, heated for 3 h after injection. Sol parameters are described in the text.

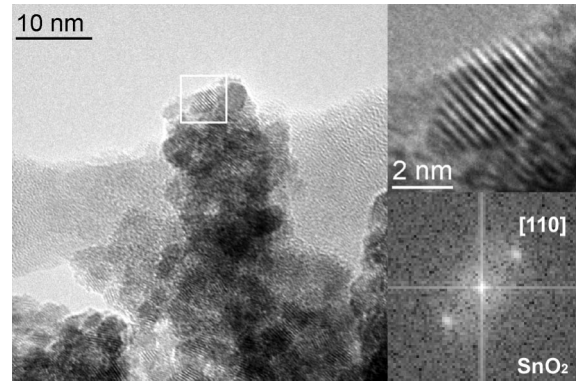


**Figure 4.** General view, HRTEM image, and power spectra of $SnO_2$ nanocrystals, heated for 3 h after injection. Sol parameters are described in the text.

(ii) Amine Concentration and the Amine Alkyl Chain Length. The amines display a catalytic activity of inorganic condensation reactions, classically[36] interpreted in terms of the deprotonation of M−OH bonds, where M is

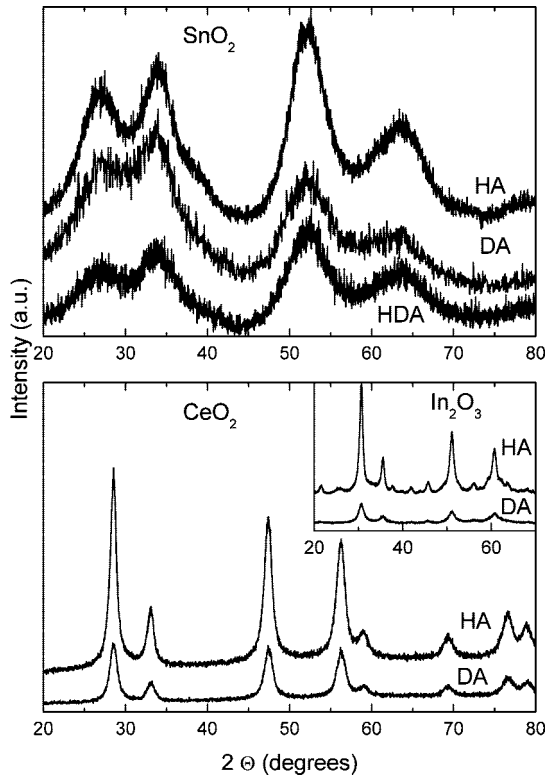


**Figure 5.** XRD patterns recorded on $SnO_2$ and $CeO_2$ nanocrystals, synthesized with the indicated amines in concentrations equivalent to $V_{DA} = 1$ and heated for 3 h after injection. The sol preparation parameters were $R_W = 16$ for $SnO_2$ and $R_{ac} = 3$, $R_B = 0.6$ for $CeO_2$ nanocrystals. In the inset, the XRD patterns are reported for $In_2O_3$ nanocrystals prepared with the indicated amines and heating for 1 h at 140 °C after injection. The sol preparation parameters were $R_{ac} = 3$ and $R_B = 4.2$.

a metal, forming strong nucleophiles that attack other M−OH species

$$\text{amine} + \text{M}-\text{OH} \rightarrow [\text{amineH}]^+ + \text{M}-\text{O}^-$$

$$\text{M}-\text{O}^- + \text{M}-\text{OH} \rightarrow -\text{M}-\text{O}-\text{M} + \text{OH}^-$$

We have seen (previous section) that this process does not proceed indefinitely after injection. The arresting time and the related nanocrystals size will be defined by the simultaneous occurring of several phenomena, such as the surface ligation by amine and the early formation of isolated regions of the injected sol in the amine/tetradecene solution. A prediction is not straightforward in these conditions. No clear trend was indeed obtained when investigating the amine concentration. The effect of the amine alkyl chain length was also investigated. The sol synthesis parameters were $R_W = 16$ for the $SnO_2$ sol and $R_{ac} = 3$, $R_B = 0.6$ for the $CeO_2$. Different amines were used in a concentration equivalent to $V_{DA} = 1$. The corresponding XRD patterns are displayed in Figure 5. In the case of $SnO_2$, the patterns provide a size increasing from 1.2 nm for DA and HDA to 1.7 nm for HA. Moreover, in Figure S2 of the Supporting Information, a similar comparison is reported for sols prepared with $R_W = 64$, where an identical trend is seen but the size differences are even more remarked, going from 1.5 to 1.9 to 2.6 nm when going from HDA to DA to HA, respectively. The $CeO_2$ size increased from 8.6 to 10 nm when using HA instead of DA. Finally, in the inset, the XRD patterns are reported for $In_2O_3$ nanocrystals prepared with the sol of Table 1, the indicated amines, and heating for 1 h at 140 °C after injection.

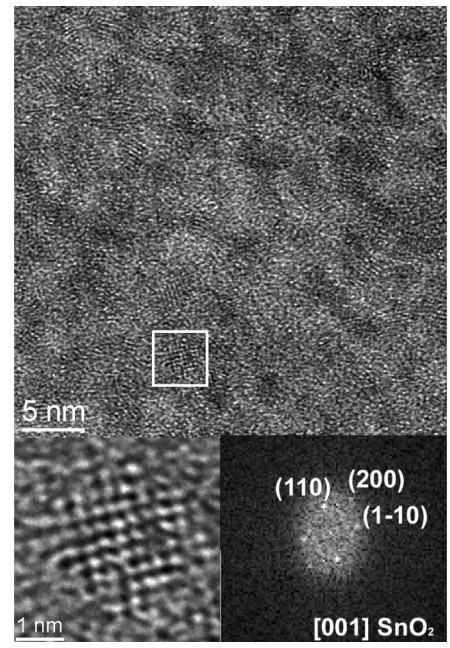


**Figure 6.** General view, HRTEM image, and power spectra of $SnO_2$ nanocrystals, synthesized with HDA and with a starting sol prepared with $R_W = 16$. The sample was heated for 3 h after injection.

A striking difference is seen, with the $In_2O_3$ nanocrystal size going from 6.3 to 11 nm when using HA instead of DA. In Figure 6, the results of a HRTEM investigation of the $SnO_2$ nanocrystals prepared with HDA are reported, in order to have an independent analysis of such small structures. $SnO_2$ nanocrystals are clearly seen, with a mean size of 2.2 ± 0.2 nm, giving a more realistic estimate with respect to the size deduced from the XRD patterns.

The influence of the amine structure on the nanocrystal size is clear, with shorter amines that result in larger particle size. On the basis of the previous considerations, the origin of this effect cannot be attributed only to steric factors because of the surface bonding, but the amine effect in determining the size and structure of the sol regions formed upon injection should also be kept into account.

(iii) Processing of the Starting Sol. In classical sol−gel processing, the structure of the species in the sol determines the structural, textural, and morphological properties of the final gel. In our process, analogously to the bulk counterpart, the final nanogels constituting the product are expected to be influenced by the processing of the starting sol. The sol processing was then modified with the aim of changing the extent of the condensation reactions: chloride-based sols were processed with different water concentrations, while the nitrate-derived sols were prepared by changing the ammonia and/or the acacH concentration.

Although both procedures were based on the shift of the condensation equilibrium toward the products, in the latter case, the decreased sol stability with increased ammonia concentration, eventually resulting in fast precipitation, was an immediate demonstration of the presence of differently

(36) Brinker, C. J.; Scherer, G. W. *Sol−Gel Science−The Physics and Chemistry of Sol−Gel Processing*; Academic Press: San Diego, CA, 1990; Chapters 2−3.

favored condensation reactions, even though a precise structural determination of the species in the sol appears as an extremely complex task. In the case of $SnO_2$, instead, there was a more straightforward way to evaluate the influence of water concentration on the sol structure, by $^{119}Sn$ NMR spectroscopy. The results of the analysis of sols prepared with various $R_W$ values are reported in the Supporting Information (Figure S3). The $^{119}Sn$ NMR spectrum of the reference sample ($SnCl_4 \cdot 5H_2O$, 2 mM) shows an intense signal at $\delta = -605$ attributable to the $^{119}Sn$ atom in a tetrahedral chorine environment. The $^{119}Sn$ NMR spectrum of the sol with $R_W = 0$ shows the same intense signal as the reference sample and a new broadband around $\delta = -590$, probably related to the solvolysis product. The spectra acquired from solutions with different $R_W$ values are similar to that of the water-free sample, although the spectrum of the solution with $R_W = 64$ seems to develop more clearly a smooth band around $\delta = -560$. This new band would be related to the formation of hydrolysis products involving Sn−O bonds. Data obtained from the sample with $R_W = 128$ confirm the hypothesis, since the spectrum shows an enhanced broad signal at $\delta = -566$. Therefore, we can propose that this signal is related to the existence of Sn−O bonds. The bandwidth can be explained on the basis of a slow hydroxyl groups exchange and also to the existence of oligomeric species (involving Sn−O−Sn). This is an important point related to the nature of the sols that are prepared for injection. Just because the condensation reactions are hindered, the term "sol" must be considered in a broad sense, as a suspension of species with a variable density and structure, going from dense colloids to poorly dense, oligomeric species, as in the case of the $SnO_2$ sols just described. Indeed, in classical works about the hydrolysis of titanium alkoxide acetylacetonato and other complexes,[37] it was shown that the base addition results in a whole range of structures, with a variable density from fractal clusters to dense particles. Moreover, in our previous work,[34] we presented a series of FTIR spectra measured on various metal oxide "sols" just displaying the variable degree of inorganic cross-linking, depending on the specific system. Finally, we have carried out in a previous work[38] a FTIR investigation in the case of $In_2O_3$, showing the presence of vibrational modes of the oxide network together with the bands of the indium acetylacetonato complex. From the whole of these results and literature data, we have defined the meaning of the term "sol" that we have been using throughout the paper.

The effect of sol processing on the final product was investigated by preparing sols with different $R_W$ and $R_B$ values (a fixed value of $R_{ac} = 0.6$ was kept for the $CeO_2$ sols), and the XRD patterns measured on the resulting products are reported in Figure 7. Syntheses were carried out with $V_{DA} = 1$ and a heating time of 3 h. The $CeO_2$ sol prepared with $R_B = 16.8$ required the addition of 1.5 mL of concentrated nitric acid for dissolving the precipitate formed upon the ammonia solution addition.

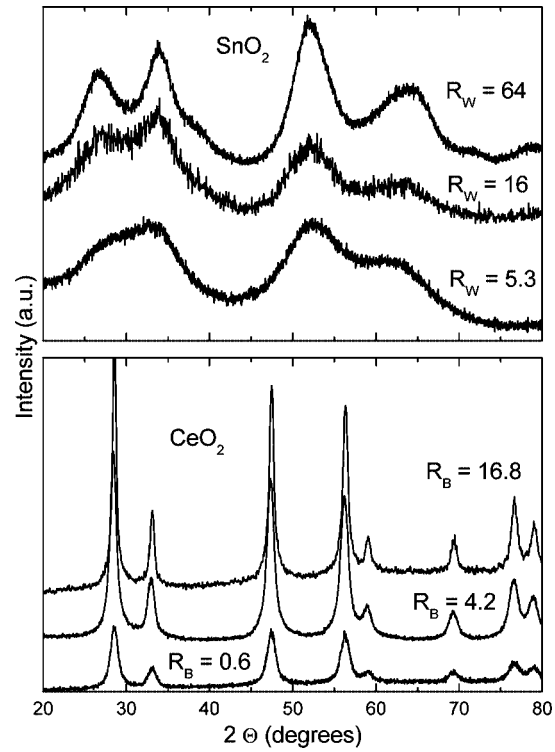


**Figure 7.** XRD patterns recorded on $SnO_2$ and $CeO_2$ nanocrystals, synthesized with the indicated sol preparation parameters. The $CeO_2$ sols were prepared with $R_{ac} = 0.6$. The injection was carried out with $V_{DA} = 1$.

In the case of $SnO_2$, the effect of the water concentration is evident first in the crystallization quality, since for $R_W = 5.3$ the nanoparticles still display an XRD pattern typical of a poorly crystallized phase, with extremely broad and not completely resolved peaks. With increasing the $R_W$ value, crystallization improves and the particle size increases from 1.2 to 1.9 nm by changing $R_W$ from 16 to 64. So the $R_W$ value influences the presence of condensed species in the starting sol, as seen before from the NMR data. After injection, if the water concentration is too low, the sol−gel transition itself will be strongly hindered. In the case of $CeO_2$, nanocrystalline products are present for every $R_B$ value, and the size increases from 8.6 to 9.8 to 17 nm when changing $R_B$ from 0.6 to 4.2 to 16.8. These results are the straightforward confirmation of what could reasonably seem still a naïve prediction: larger oxide species in the starting sol will condense to larger final nanoparticles. In Figure S4 of the Supporting Information, similar results are presented for $In_2O_3$ nanocrystals, but in that case, an effective size increase occurs only with $R_B = 16.8$, whereas for lower $R_B$ values, the size increases only slightly: the modulation of the initial sol processing introduces modifications in the surface chemistry of the sol species, depending on the hydrolytic chemistry of each system, and resulting in different size of the final nanocrystal as a function of $R_B$. For completeness, in Figure S5 of the Supporting Information, a representative TEM image of the $In_2O_3$ sample prepared with $R_B = 4.2$ is presented.

(37) (a) Doeuff, S.; Henry, M.; Sanchez, C.; Livage, J. *J. Non-Cryst. Solids* **1987**, *89*, 206–216. (b) Livage, J.; Henry, M.; Sanchez, C. *Prog. Inorg. Chem.* **1988**, *18*, 259–341. (c) Henry, M.; Jolivet, J. P.; Livage, J. *Structure and Bonding*; Springer-Verlag: Heidelberg, Germany, 1992; Vol. 77, pp 153−206. (d) Sanchez, C.; Livage, J.; Henry, M.; Babonneau, F. *J. Non-Cryst. Solids* **1988**, *100*, 65–76. (e) Leaustic, A.; Babonneau, F.; Livage, J. *Chem. Mater.* **1989**, *1*, 248–252. (f) Kallala, M.; Sanchez, C.; Cabane, B. *Phys. Rev. E* **1993**, *48*, 3692–3704. (g) Blanchard, J.; Ribot, F.; Sanchez, C.; Bellot, P.-V.; Trokiner, A. *J. Non-Cryst. Solids* **2000**, *265*, 83–97.

(38) Epifani, M.; Diaz, R.; Arbiol, J.; Siciliano, P.; Morante, J. R. *Chem. Mater.* **2006**, *18*, 840–846.

*(c) Notes about the Chemical Composition of the Nanocrystals.* The characterization of the nanocrystals was completed by analyzing the consistence of the organic residuals after the synthesis. The as-prepared $SnO_2$ nanocrystals contained 2.52, 14.58, and 4.06% of N, C, and H, respectively, whereas the values for $CeO_2$ were 1.77, 4.36, and 1.04%, respectively. The samples were prepared with the same synthesis parameters related to Figure 1. The concentrations do not indicate an excessive organic contamination due to the synthesis process. The found values are in agreement with the presence of residuals just because of the expected bonding of amine to the nanoparticles surface. There is a higher concentration in the case of $SnO_2$, probably due to the residual alkoxy groups and larger amount of methanol residuals. For completeness, the heat-treated $SnO_2$ nanocrystals were analyzed by XPS, in order to reveal the presence of residual chlorine. The results are shown in the Supporting Information, showing that the organic and chlorine residuals are removed after heat treatment at 500 °C. The quantitative determination gives a 0.2% C atomic concentration, including the adventitious contamination. A similar result is shown for $In_2O_3$ nanocrystals heat-treated in similar conditions.

## Conclusions

Metal oxide nanoparticles can be prepared by injecting metal oxide sols in a coordinating environment containing an alkylamine. The sols are prepared in such a way to hinder the condensation reactions, which requires the term "sol" to be meant in a broad sense as concerns the structure of the metal oxide species. The pathway leading from the starting sol to the final nanoparticles displays the following features:

(1) The process has an applicability that comes from the wide range of conditions favoring the hydrolysis of metal ions; that metal oxide nanocrystals can be effectively prepared must be verified in each case, due to kinetic factors that can prevent crystallization.

(2) The particle formation kinetics is very fast and for some systems results in a crystalline product after a few minutes of processing; the growth time is not a critical parameter after a minimum crystallization threshold time is reached.

(3) The alkyl chain length of the amine influences the final nanocrystal size, with bulkier amines resulting in smaller nanocrystals;

(4) The sol preparation parameters influence the final nanocrystal size, with larger nanocrystals resulting from sols prepared with more favored condensation reactions.

**Acknowledgment.** This work was supported by the European Union in the frame of the NANOS4 (Grant NMP4-CT-2003-001528) project. We thank the XRD, FTIR, organic elemental analysis unit of the Serveis Cientificotècnics de la Universitat de Barcelona and the Servei de Resonància Magnètica Nuclear of the University of Barcelona for their cooperation; MATGAS 2000 AIE for the provision of their facilities; and Dr. Pau Solsona for technical assistance in the BET experiments. We thank Teresa Andreu for the support during the characterization of the materials.

**Supporting Information Available:** Details on the phase composition of several systems; $^{1}H$ NMR spectra on the synthesis liquid byproduct; $^{119}Sn$ NMR spectra on $SnO_2$ sols; further XRD patterns on $SnO_2$, $CeO_2$, and $In_2O_3$ nanocrystals; TEM of $In_2O_3$ nanocrystals; XPS survey spectra of $SnO_2$ and $In_2O_3$ samples (PDF). This material is available free of charge via the Internet at http://pubs.acs.org.

CM803282K